



JUNE 29 2023

# A three-dimensional active cloaking strategy for the Helmholtz equation that exploits the symmetry of the platonic solids

Cheuk-Him Yeung; William J. Parnell ; Tom Shearer 



*JASA Express Lett* 3, 063601 (2023)

<https://doi.org/10.1121/10.0019906>



View  
Online



Export  
Citation

CrossMark





**ASA**

Advance your science and career as a member of the  
**Acoustical Society of America**

[LEARN MORE](#)

# A three-dimensional active cloaking strategy for the Helmholtz equation that exploits the symmetry of the platonic solids

Cheuk-Him Yeung, William J. Parnell,  and Tom Shearer<sup>a)</sup> 

Department of Mathematics, University of Manchester, Manchester, M13 9PL, United Kingdom

[cheukhim.yeung@manchester.ac.uk](mailto:cheukhim.yeung@manchester.ac.uk), [william.parnell@manchester.ac.uk](mailto:william.parnell@manchester.ac.uk), [tom.shearer@manchester.ac.uk](mailto:tom.shearer@manchester.ac.uk)

**Abstract:** An active cloaking strategy for the scalar Helmholtz equation in three dimensions is developed by placing active sources at the vertices of Platonic solids. In each case, a “silent zone” is created interior to the Platonic solid and only the incident field remains in a defined region exterior to this zone. This distribution of sources ensures that implementation of the cloaking strategy is efficient: once the multipole source amplitudes at a single source location are determined, the other amplitudes are calculated by multiplying the multipole source vector by a rotation matrix. The technique is relevant to any scalar wave field. © 2023 Author(s). All article content, except where otherwise noted, is licensed under a Creative Commons Attribution (CC BY) license (<http://creativecommons.org/licenses/by/4.0/>).

[Editor: Siu-Kit Lau]

<https://doi.org/10.1121/10.0019906>

**Received:** 21 April 2023 **Accepted:** 12 June 2023 **Published Online:** 29 June 2023

## 1. Introduction

Over the last two decades, excitement has been generated around the idea of rendering objects invisible to incident excitation (Miller, 2006; Norris, 2008; Schurig *et al.*, 2006), via passive (Cai *et al.*, 2007; Silveirinha *et al.*, 2007; Zhang *et al.*, 2011) or active (Miller, 2006; Vasquez *et al.*, 2009a; Zheng *et al.*, 2010) cloaking. The latter employs sources to suppress fields and has been of interest since Lueg’s patent in 1936 (Guicking, 1990). Significant work on anti-sound/anti-vibration has been carried out since then (Cheer, 2016; Fuller *et al.*, 1996; Guicking, 2007; Nelson and Elliott, 1991). Specific choices for the active sources ensure quiet zones and illusions (Ma *et al.*, 2013; Zheng *et al.*, 2010) and control arrangements can be optimised to reduce acoustic scattering in a stationary fluid (Egler *et al.*, 2019a; House *et al.*, 2020; Lin *et al.*, 2021; O’Neill *et al.*, 2015) and in a convected flow field (Egler *et al.*, 2019b).

Recent interest has centred on object-independent active cloaking methods, e.g., Miller’s sensing method (Miller, 2006). This approach cannot provide a relationship between the incident field and source amplitudes however, so this was addressed in (Vasquez *et al.*, 2009a,b, 2011), using multipole sources to create silent zones in two dimensions (2D). Further progress came in (Norris *et al.*, 2012), where closed-form explicit formulas for the active source coefficients were deduced. This was also extended to elastodynamics (Futhazar *et al.*, 2015; Norris *et al.*, 2014). This approach is attractive because the active source coefficients are independent of the object to be cloaked. This is in contrast to object-dependent approaches, which must be modified in resonant regimes (O’Neill *et al.*, 2016). The latter approach, however, does not suffer from large amplitudes in the vicinity of the active source regions.

Although there has been extensive work on active manipulation of sound in three dimensions (3D) (Ahrens, 2012; Egarguin *et al.*, 2020; Elliott *et al.*, 2012; Onofrei and Platt, 2018), the object-independent approach has thus far been conducted in 2D only, with the sole exception of Vasquez *et al.* (2013), which considered the Helmholtz equation in 3D, where results were provided for the case of four active sources.

Here, we provide a framework for active cloaking in 3D. We derive expressions for the active source coefficients and introduce a fast, efficient methodology by placing active sources on vertices of the Platonic solids and exploiting their symmetry. Regardless of the incident field, once active source coefficients have been deduced for *one* of the active sources, the remaining source amplitudes can subsequently be determined, thus providing a complete exposition of 3D active cloaking for the Helmholtz equation.

## 2. Methodology

We consider active exterior cloaking for time-harmonic waves (with dependence  $e^{-i\omega t}$ , where  $\omega$  is the angular frequency and  $t$  is time) governed by the 3D, homogeneous Helmholtz equation  $(\nabla^2 + k^2)u(\mathbf{x}) = 0$ , where

<sup>a)</sup>Also at: Department of Materials, University of Manchester, Manchester, M13 9PL, UK.

$k = \omega/c$  is the wavenumber, with  $c$  the wavespeed. For acoustics, the scalar field  $u(\mathbf{x})$  is the velocity potential at  $\mathbf{x} = (x, y, z)$ .

Figure 1 illustrates the case when a planar incident field  $u_i(\mathbf{x})$  is acted on by the active field  $u_d(\mathbf{x})$  generated by  $L$  multipole active sources. The field subsequently scattered from an object interior to the active field is denoted by  $u_s(\mathbf{x})$ . These fields are

$$u_i(\mathbf{x}) = e^{i\mathbf{k}\cdot\mathbf{x}} = \sum_{n=0}^{\infty} \sum_{m=-n}^n Q_{nm} U_n^m(\mathbf{x}), \tag{1}$$

$$u_d(\mathbf{x}) = \sum_{\ell=1}^L \sum_{n=0}^{\infty} \sum_{m=-n}^n q_{\ell,nm} V_n^m(\mathbf{x} - \mathbf{x}_{\ell}), \tag{2}$$

$$u_s(\mathbf{x}) = \sum_{n=0}^{\infty} \sum_{m=-n}^n a_{nm} V_n^m(\mathbf{x}), \tag{3}$$

where  $U_n^m(\mathbf{x}) = j_n(k|\mathbf{x}|)Y_n^m(\hat{\mathbf{x}})$  and  $V_n^m(\mathbf{x}) = h_n^{(1)}(k|\mathbf{x}|)Y_n^m(\hat{\mathbf{x}})$  are incoming and outgoing spherical waves, respectively (Martin, 2006), noting that  $j_n(k|\mathbf{x}|)$  is the spherical Bessel function of the first kind and  $h_n^{(1)}(k|\mathbf{x}|)$  is the spherical Hankel function of the first kind. Further,  $Y_n^m(\hat{\mathbf{x}}) = A_n^m P_n^m(\cos \theta)e^{im\varphi}$  is the normalized spherical harmonic function, where the hat denotes a unit vector,  $P_n^m(\cos \theta)$  is the associated Legendre function of order  $m$  and degree  $n$  in terms of the polar angle  $\theta$  and the azimuthal angle  $\varphi$  and

$$A_n^m = \sqrt{\frac{2n+1}{4\pi} \frac{(n-m)!}{(n+m)!}} \tag{4}$$

Referring to Fig. 1, we write  $\mathbf{k} = k\hat{\mathbf{k}}$  where  $\hat{\mathbf{k}} = (\sin \theta_i \cos \varphi_i, \sin \theta_i \sin \varphi_i, \cos \theta_i)$  is the unit propagating vector, where  $\theta_i$  and  $\varphi_i$  are the incident wave angles. For plane wave incidence, the expansion coefficients  $Q_{nm} = 4\pi i^n \overline{Y_n^m(\hat{\mathbf{k}})}$  thus depend only on these incident angles, with overline denoting complex conjugation. For other types of incident fields, the values of  $Q_{nm}$  would be different, but the rest of the methodology presented below would be unchanged. The amplitude of the radiation mode with order  $(n, m)$  in the  $\ell$ th active source (which is located at  $\mathbf{x}_{\ell}$ ) is  $q_{\ell,nm}$ , where  $\ell = 1, 2, \dots, L$  and  $a_{nm}$  is the scattering coefficient of the object.

To achieve active cloaking,  $q_{\ell,nm}$  are sought such that for some closed domain  $C$  surrounded by the active sources with  $\mathbf{x}_{\ell} \notin C$ , we have  $u_i(\mathbf{x}) + u_d(\mathbf{x}) = 0$  for  $\mathbf{x} \in C$  and  $u_d(\mathbf{x}) \rightarrow 0$  as  $|\mathbf{x}| \rightarrow \infty$ . Thus, while the scattered field from any object is nullified in  $C$ , we also stipulate that the radiation of  $u_d$  itself to the far field is zero, leaving minimal evidence of the cloak.

The active sources are located at the vertices of an imaginary Platonic solid, thus limiting the number of sources  $L$  to five values (Euclid, 2012) [see Figs. 2(a)–2(e)]. This geometry ensures that the sources reside on the circumsphere of the Platonic solids such that  $|\mathbf{x}_{\ell}| = x_0$  for all  $\ell$  in each case, where  $x_0$  is an arbitrary constant. We set  $\mathbf{x}_1 = (0, 0, -x_0)$  in every case such that the active source with  $\ell = 1$  always has the lowest  $z$ -coordinate. To locate the remaining sources, we note that a Platonic solid consisting of  $q$   $p$ -sided regular polygonal faces around each vertex can be characterized by two indices  $(p, q)$  [e.g., a cube with three squares around each vertex has the indices  $(4, 3)$ ]. We define the length of each side of a Platonic solid as  $sx_0$ .

The position of each active source is determined from  $(p, q)$  and  $s$ , whose values are listed in Table 1 (see Part 2 of the supplementary material<sup>1</sup>). Since the source distribution is  $q$ -fold rotationally symmetric about the  $z$ -axis, if we assign

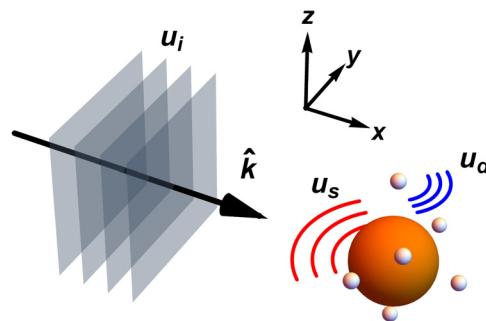


Fig. 1. In the active cloaking problem, the incident plane wave  $u_i$  (propagating in the direction  $\hat{\mathbf{k}}$ ) impinges upon an object (the orange sphere here) and is scattered ( $u_s$ ). The amplitudes of the  $L$  active sources (smaller spheres) produce the active field  $u_d$ , nullifying  $u_i$  in a region containing the object, thus cancelling the scattered field.

Table 1. Geometric properties of the Platonic distributions of active sources and the volumes of the cloaked regions  $\mathcal{V} = |C|$  (to four decimal places) when the radius  $a$  takes the lower limit in Eq. (10). Here,  $\phi = (1 + \sqrt{5})/2$ .

$L$	$(p, q)$	$s$	$\mathcal{V}$ (in units of $x_0^3$ )
4	(3, 3)	$2\sqrt{6}/3$	0.0033
6	(3, 4)	$\sqrt{2}$	0.0675
8	(4, 3)	$2\sqrt{3}/3$	0.0538
12	(3, 5)	$2\sqrt{5}(3 - \phi)/5$	0.4562
20	(5, 3)	$2\sqrt{3}(\phi - 1)/3$	0.3692

the indices  $\ell = 2, \dots, q + 1$  to the  $q$  vertices located immediately above the source  $\ell = 1$  in the counterclockwise direction, their position vectors  $\mathbf{x}_\ell$  are given by

$$\mathbf{x}_\ell = x_0(r_2 \cos \varphi_\ell, r_2 \sin \varphi_\ell, z_2), \tag{5}$$

where  $z_2 = (s^2 - 2)/2$ ,  $r_2 = \sqrt{1 - z_2^2}$  and  $\varphi_\ell = 2(\ell - 2)\pi/q$ .

We note that, although the active sources are arranged symmetrically on the vertices of the Platonic solids, the incident wave breaks this symmetry, and therefore, different values of  $q_{\ell, nm}$  are required for each source. To determine  $q_{\ell, nm}$  and the geometric shape of the cloaked region  $C$ , we employ the procedure from Vasquez *et al.* (2013) as the starting point and use the approach in Norris *et al.* (2012) to obtain explicit expressions (see Part 1 of the supplementary material<sup>1</sup>) in the form

$$q_{\ell, nm} = -ik^2 \sum_{t=0}^{\infty} \sum_{s=-t}^t Q_{ts} q_{\ell, nm, ts}, \tag{6}$$

$$q_{\ell, nm, ts} = \sum_{\nu=0}^{\infty} \sum_{\mu=-\nu}^{\nu} \widehat{S}_{t\nu}^{s\mu}(\mathbf{x}_\ell) D_{\nu n} \mathcal{F}_{n\nu}^{m\mu}(\mathbf{x}_\ell, \partial C_\ell). \tag{7}$$

We note that the expression for  $q_{\ell, nm}$  depends on the orientation of the incoming wave via  $Q_{ts}$  and is, therefore, valid for any angles of incidence. In Eq. (7),  $\widehat{S}_{t\nu}^{s\mu}(\mathbf{x}_\ell)$  [defined in Eqs. (8)–(11) of the supplementary material<sup>1</sup>] is a coefficient depending on the position vector  $\mathbf{x}_\ell$ , and the quantities  $D_{\nu n}$ ,  $\mathcal{F}_{n\nu}^{m\mu}(\mathbf{x}_\ell, \partial C_\ell)$  are

$$D_{\nu n} = j_\nu(kax_0) j_n'(kax_0) - j_\nu'(kax_0) j_n(kax_0), \tag{8}$$

$$\mathcal{F}_{n\nu}^{m\mu}(\mathbf{x}_\ell, \partial C_\ell) = \int_{\partial C_\ell} \overline{Y_n^m(\mathbf{y} - \mathbf{x}_\ell)} Y_\nu^\mu(\mathbf{y} - \mathbf{x}_\ell) dS(\mathbf{y} - \mathbf{x}_\ell), \tag{9}$$

where a prime denotes the derivative with respect to the argument, and finally

$$\frac{s}{2 \sin(\pi/p)} \leq a < 1 \tag{10}$$

(see Part 2 of the supplementary material<sup>1</sup>). The surface integral  $\mathcal{F}_{n\nu}^{m\mu}$  is evaluated over the face  $\partial C_\ell$  and parameterized by the vector  $\mathbf{y} - \mathbf{x}_\ell$  for  $\mathbf{y} \in \partial C_\ell$ . It appears that an explicit form of  $\mathcal{F}_{n\nu}^{m\mu}$  is not available; however, the integral can be simplified such that its numerical evaluation becomes significantly less expensive (see Part 4 of the supplementary material<sup>1</sup>). The formulations in Eqs. (6)–(10) hold when the domain  $C$  is completely bounded by the union of faces  $\partial C_\ell$ , where  $\ell = 1, 2, \dots, L$ , and  $|\mathbf{y} - \mathbf{x}_\ell| = ax_0$  for  $\mathbf{y} \in \partial C_\ell$  such that  $\partial C_\ell$  is a surface belonging to a sphere centered at  $\mathbf{x}_\ell$  with radius  $ax_0$ . The cloaked region  $C$  therefore consists of the domain interior to the union of surfaces formed by identical imaginary spheres of radius  $ax_0$  located at the vertices and the source amplitude in the form of Eqs. (6)–(10) applies to a general incident wave. The case of plane wave incidence [ $Q_{nm} = 4\pi i^n Y_n^m(\widehat{\mathbf{k}})$ ] admits the following compact form:

$$q_{\ell, nm} = -ik^2 e^{i\mathbf{k} \cdot \mathbf{x}_\ell} \sum_{\nu=0}^{\infty} \sum_{\mu=-\nu}^{\nu} Q_{\nu\mu} D_{\nu n} \mathcal{F}_{n\nu}^{m\mu}(\mathbf{x}_\ell, \partial C_\ell). \tag{11}$$

For computational purposes, the infinite series in Eq. (11) needs to be truncated. In Part 3 of the supplementary material<sup>1</sup> we discuss how to choose this truncation parameter such that the source amplitude converges with a prescribed level of accuracy.

In Figs. 2(a)–2(e), we illustrate the respective cloaked regions inside each of the Platonic solids with  $a$  taken as the lower bound in Eq. (10) (when the volume of the domain is a maximum). In each case, the surface of integration  $\partial C_\ell$  is delimited by  $q$  identical circular arcs ( $q$  depends on  $L$  as indicated in Table 1). For non-Platonic distributions of sources, these arcs are *not* identical.

We first evaluate  $\mathcal{F}_{n\nu}^{m\mu}(\mathbf{x}_1, \partial C_1)$  for  $\ell = 1$ . A parametric form for the corresponding face  $\partial C_1$  is conveniently derived using a local spherical coordinate system centred at  $\mathbf{x}_1$  (see Part 2 of the supplementary material<sup>1</sup>). Since  $\partial C_1$

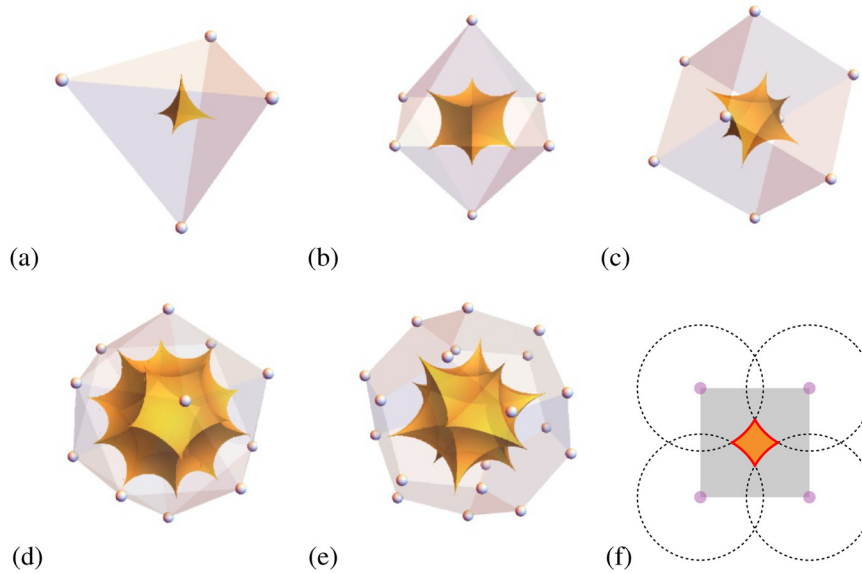


Fig. 2. In (a)–(e), the cloaked regions are illustrated for the cases of the (a) tetrahedron (four vertices), (b) octahedron (six vertices), (c) cube (eight vertices), (d) icosahedron (12 vertices), and (e) dodecahedron (20 vertices). In (f), a cross-section through the plane  $z=0$  in (b) is shown.

possesses  $q$ -fold rotational symmetry about the  $z$ -axis, it can be subdivided into  $q$  congruent segments, each being the region bounded by

$$g_\ell(\varphi) \leq \cos \theta \leq 1, \tag{12}$$

$$\varphi_\ell - \pi/q \leq \varphi \leq \varphi_\ell + \pi/q, \tag{13}$$

where

$$g_\ell(\varphi) = \left\{ 1 + \left[ a^2 h^2 \cos^4(\varphi - \varphi_\ell) - h(1 - a^2) \times \cos^2(\varphi - \varphi_\ell) \right]^{1/2} \right\} / \left\{ a[1 + h \cos^2(\varphi - \varphi_\ell)] \right\}, \tag{14}$$

$$h = (1 - z_2)/(1 + z_2), \tag{15}$$

and  $\varphi_\ell, z_2$  are defined as in Eq. (5). The surface  $\partial C_1$  is defined by the union of segments parameterized by Eqs. (12)–(15) over  $\ell = 2, \dots, q + 1$ . Since all surfaces of integration  $\partial C_\ell$  have an identical shape within each Platonic distribution of sources, this parametric form describes not only the face  $\partial C_1$  but also all other faces provided a suitable coordinate transformation is applied to account for orientation. In Table 1, we state the volume  $\mathcal{V} = |C|$  of the cloaked region  $C$  by using the divergence theorem on Eqs. (12)–(15).

Given the regularity and rotational symmetry of the Platonic source distribution, we determine the amplitudes of all sources using only the knowledge of the formula from Eq. (11) and the integral  $\mathcal{I}_{nv}^{m\mu}(\mathbf{x}_1, \partial C_1)$ , avoiding the integrations for all  $L$  active sources. We write the coefficient  $q_{\ell, nm}$  as  $q_{\ell, nm}(\hat{\mathbf{k}}, \mathbf{x}_\ell, \partial C_\ell)$  to indicate its dependence on the propagating vector  $\hat{\mathbf{k}}$  and the two geometric parameters. For brevity, we also denote the surface integral as  $\mathcal{I}_\ell$  by suppressing indices and arguments in Eq. (9). Define a new coordinate system  $\mathbf{x}' = (x', y', z') = \mathbf{R}(\hat{\mathbf{v}}, \Theta)\mathbf{x}$  where  $\mathbf{R}(\hat{\mathbf{v}}, \Theta)$  is a rotation matrix, with  $\hat{\mathbf{v}}$  being the unit vector representing the rotation axis and  $\Theta$ , the rotation angle. As illustrated in Fig. 3, we rotate the

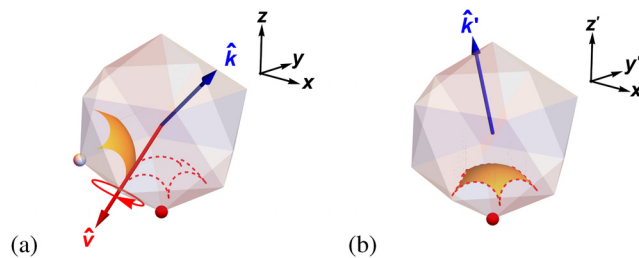


Fig. 3. Transformation between (a) the original space  $\mathbf{x} = (x, y, z)$  and (b) the rotated space  $\mathbf{x}' = (x', y', z')$ . The rotation  $\mathbf{R}(\hat{\mathbf{v}}, \Theta)$  maps the  $\ell$ th active source to the bottom-most position in the source distribution, replacing the source  $\ell = 1$  (the red sphere) with the white sphere. The incident propagating vector  $\hat{\mathbf{k}}$  maps to  $\hat{\mathbf{k}}'$ .

original frame  $\mathbf{x}$  such that in the rotated frame  $\mathbf{x}'$ , the  $\ell$  th active source, takes the bottom-most location, replacing the source  $\ell = 1$ , and the corresponding bounding surface  $\partial C_\ell$  has the same orientation as  $\partial C_1$  in the original frame  $\mathbf{x}$ . Under this transformation, the amplitude in Eq. (11) becomes

$$q'_{\ell,nm}(\widehat{\mathbf{k}}', \mathbf{x}'_\ell, \partial C'_\ell) = -ik^2 e^{ik\widehat{\mathbf{k}}' \cdot \mathbf{x}'_\ell} \sum_{\nu=0}^{\infty} \sum_{\mu=-\nu}^{\nu} Q'_{\nu\mu} D'_{\nu n} \mathcal{J}'_\ell, \tag{16}$$

where  $\widehat{\mathbf{k}}'$ ,  $\mathbf{x}'_\ell$ , and  $\partial C'_\ell$  are the new forms of the propagating vector, position vector, and integration surface in the space  $\mathbf{x}'$ , respectively, and  $Q'_{\nu\mu} = 4\pi i^\nu Y'_\nu^\mu(\widehat{\mathbf{k}}')$ . By construction,  $\mathbf{x}'_\ell = \mathbf{x}_1$  and  $\partial C'_\ell = \partial C_1$ . As the forms of  $D_{\nu n}$  and  $\mathcal{J}_\ell$  suggest in Eqs. (8) and (9), they are independent of  $\widehat{\mathbf{k}}$ . The rotational symmetry of the Platonic solids and our choice of  $\mathbf{R}$  ensures that they remain rotationally invariant across all  $\ell$ . In particular, we have  $D'_{\nu n} = D_{\nu n}$  and  $\mathcal{J}'_\ell = \mathcal{J}_1$ . The source amplitude  $q_{\ell,nm}(\widehat{\mathbf{k}}, \mathbf{x}_\ell, \partial C_\ell)$ , is thus transformed to  $q_{1,nm}(\widehat{\mathbf{k}}', \mathbf{x}_1, \partial C_1)$  in the rotated frame. While the former is calculated by integrating over  $\partial C_\ell$  for all  $\ell$ , the latter can be evaluated by simply integrating over  $\partial C_1$  parameterized by Eqs. (12)–(15) and replacing  $\widehat{\mathbf{k}}$  by  $\widehat{\mathbf{k}}'$ . If we express the source coefficients as a vector  $\mathbf{q}_{\ell,n} = \{q_{\ell,nm}\}_{m=-n}^n$ , then it can be shown that the system of linear equations

$$\mathbf{D}^n(\gamma, \beta, \alpha) \mathbf{q}_{\ell,n}(\widehat{\mathbf{k}}, \mathbf{x}_\ell, \partial C_\ell) = \mathbf{q}_{1,n}(\widehat{\mathbf{k}}', \mathbf{x}_1, \partial C_1) \tag{17}$$

holds, where  $\mathbf{D}^n(\gamma, \beta, \alpha)$  [defined in Eqs. (103)–(105) of the supplementary material<sup>1</sup>] is the Wigner D-matrix (Wigner, 2012) with dimensions  $(2n + 1) \times (2n + 1)$  and  $\gamma, \beta, \alpha$  are the Euler angles (Varshalovich *et al.*, 1988) of the matrix  $\mathbf{R}(\widehat{\mathbf{v}}, \Theta)$  such that

$$\mathbf{R}(\widehat{\mathbf{v}}, \Theta) = \mathbf{R}(\widehat{\mathbf{e}}_z, \gamma) \mathbf{R}(\widehat{\mathbf{e}}_y, \beta) \mathbf{R}(\widehat{\mathbf{e}}_z, \alpha), \tag{18}$$

with  $\widehat{\mathbf{e}}_y, \widehat{\mathbf{e}}_z$  being the unit vectors along the  $y$  and  $z$  axes. By solving Eq. (17) for  $n = 0, 1, \dots, N$  with  $N$  a positive integer, we can retrieve the full set of amplitudes  $q_{\ell,nm}(\widehat{\mathbf{k}}, \mathbf{x}_\ell, \partial C_\ell)$  up to the  $N$ th order multipole. The cloaking device is thus devised by repeating this procedure with the corresponding  $\widehat{\mathbf{k}}$  and Euler angles for each source. Employing active sources on the vertices of the Platonic solids is beneficial because once one set of source coefficients is determined, those for the others follow from simple post-processing operations. See Part 5 of the supplementary material<sup>1</sup> for more details, including the exact form of the rotation matrix  $\mathbf{R}$ .

### 3. Results

The method is illustrated in Fig. 4, with  $L=20$  active sources distributed at the vertices of a regular dodecahedron with source distance  $kx_0 = 5\pi$ , which was produced using a Mathematica code that is available to download from [https://github.com/himyung1025/3d\\_silent\\_zone\\_cloaking](https://github.com/himyung1025/3d_silent_zone_cloaking). We consider the problem in the context of acoustics, but the principles are similar for other scalar waves. In Figs. 4(a)–4(d), the incident plane wave propagates in the positive  $x$  direction with  $\theta_i = \pi/2, \varphi_i = 0$ ; in Fig. 4(e)–4(h), it has angles of incidence  $\theta_i = \pi/2, \varphi_i = \pi/4$ . In Figs. 4(a), 4(b), 4(e), and 4(f), the scattering object inside the cloaked region  $C$  is a sound-soft sphere with radius  $kA = 3(1 - a)kx_0 \approx 0.8579\pi$ , where  $a = (2\sqrt{6}/3)/[2\sin(\pi/3)]$ , and  $a$  is chosen to be the minimum permissible radius of the imaginary spheres bounding  $C$  for  $L=4$ , which means that the scattering sphere has a radius three times that of the inscribed sphere of  $C$  when  $L=4$ . In

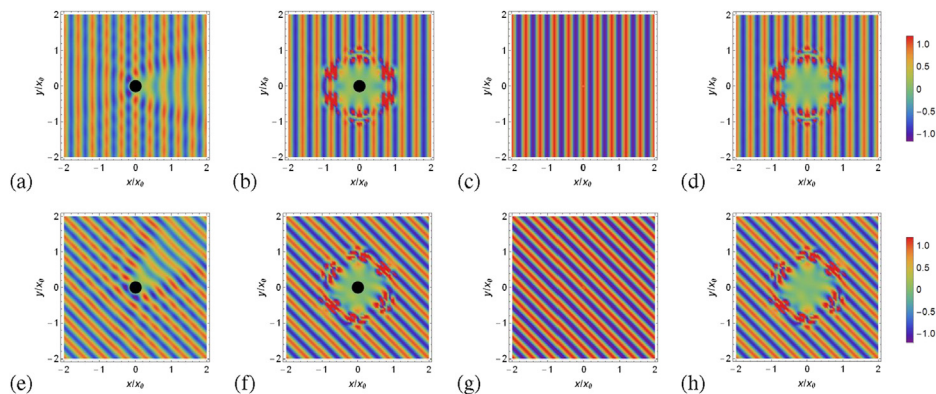


Fig. 4. The real part of the total wave field  $u$  on the cross section  $z=0$  with a sound-soft sphere subject to an incident plane wave with angles of incidence  $\theta_i = \pi/2, \varphi_i = 0$  (a)–(d) and  $\theta_i = \pi/2, \varphi_i = \pi/4$  (e)–(h) when the cloaking devices are switched off (a), (c), (e), (g) and on (b), (d), (f), (h), in the presence (a), (b), (e), (f) and absence (c), (d), (g), (h) of a scatterer. The source distance is  $kx_0 = 5\pi$  and the sphere radius is  $kA \approx 0.8579\pi$ . A total of  $L=20$  multipole active sources are used, including up to  $N=10$ .



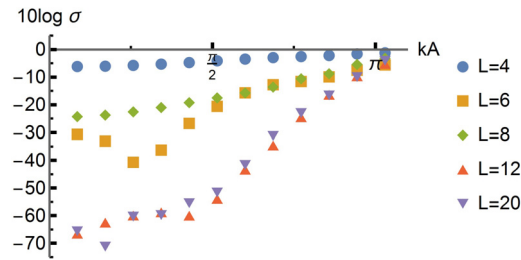


Fig. 5. The SWL for scattering from the sound-soft sphere inside the cloaked region for the five different  $L$  and  $\pi/2 \leq kx_0 \leq 6\pi$  at intervals of  $\pi/2$  (or  $0.0858\pi \leq kA \leq 1.0294\pi$  at intervals of approximately  $0.0858\pi$ ). Other parameters are the same as in Fig. 4.

Figs. 4(c), 4(d), 4(g), and 4(h), we show the case where there is no scattering object. In all subplots, the real part of the total wave field  $u$  on the cross-section  $z=0$  is shown. In Figs. 4(a), 4(c), 4(e), and 4(g), the cloaking devices are inactive and a prominent scattering pattern, including distorted wavefronts and a shadow region behind the sphere, is observed. In Figs. 4(b), 4(d), 4(f), and 4(h), the cloaking devices are activated and the multipole order of each active source is taken as  $N=10$ . The series expansions for the source coefficients in Eq. (11) are truncated such that the active field produced by each source is within 1% relative error. The spheres now reside in quasi-silent regions. The straighter wavefronts and the absence of the shadow region in the figures indicate that the incident wave is scattered only slightly by the sphere inside the quiet zone and the sources radiate little into the exterior of the silent region, demonstrating the cloak’s effectiveness. The wave field diverges within small neighbourhoods of the active point sources. In practice, these large fields are confined within the finite-sized sources. We have cropped the plot at  $\text{Re}(u) = 1.2$ .

Global effectiveness can be assessed by defining the sound power level (SWL),

$$\text{SWL} = 10 \log \sigma, \quad \sigma = \frac{W(u_d \neq 0)}{W(u_d = 0)}. \tag{19}$$

For acoustic waves, the SWL is the ratio between the sound power  $W$  in the far field after ( $u_d \neq 0$ ) and before ( $u_d = 0$ ) cloak activation (see Part 6 of the supplementary material<sup>1</sup>). In Fig. 5, we plot the SWL in the case of scattering from a sound-soft sphere for the source distributions depicted in Fig. 2. The order  $N$ , the sphere radius  $A$  and the direction of the incident wave are as in Fig. 4.

For each  $kA$ , the truncation parameter is chosen to achieve a relative error of less than 1% in the active field generated by each source. We require  $\sigma < 1$  and thus  $10 \log \sigma < 0$ . For all cases, the SWL remains negative for the range of  $kA$  studied here with increased efficacy at lower frequencies. As the source number  $L$  increases the cloaking effect generally improves, with a maximum reduction of approximately 70 decibels achieved when  $L=20$  at  $kA \approx 0.1716\pi$ . Further parameter studies can be found in Part 6 of the supplementary material.<sup>1</sup>

#### 4. Conclusion

In conclusion, we have formulated an efficient, 3D, active exterior cloaking strategy for the scalar Helmholtz equation. The Platonic distribution of the active sources means that we only need to determine the source amplitudes at one location; those at other locations follow from post-processing, exploiting the symmetry and regularity of the Platonic solids.

#### Acknowledgments

This work was supported by a University of Manchester President’s scholarship for Yeung (2017-21) and by the Engineering and Physical Sciences Research Council (EP/L018039/1) for Parnell. The authors have no conflicts of interest to declare. The data in this paper was generated using Mathematica code that is available to download at [https://github.com/himyeung1025/3d\\_silent\\_zone\\_cloaking](https://github.com/himyeung1025/3d_silent_zone_cloaking).

#### References and links

<sup>1</sup>See supplementary material at <https://doi.org/10.1121/10.0019906> for detailed mathematical derivations of the active noise control model.

Ahrens, J. (2012). *Analytic Methods of Sound Field Synthesis* (Springer Science & Business Media, New York).  
 Cai, W., Chettiar, U. K., Kildishev, A. V., and Shalae, V. M. (2007). “Optical cloaking with metamaterials,” *Nat. Photon.* **1**(4), 224–227.  
 Cheer, J. (2016). “Active control of scattered acoustic fields: Cancellation, reproduction and cloaking,” *J. Acoust. Soc. Am.* **140**(3), 1502–1512.  
 Egarguin, N. J. A., Zeng, S., Onofrei, D., and Chen, J. (2020). “Active control of Helmholtz fields in 3D using an array of sources,” *Wave Motion* **94**, 102523.  
 Egger, D., Chung, H., Montiel, F., Pan, J., and Kessissoglou, N. (2019a). “Active noise cloaking of 2D cylindrical shells,” *Wave Motion* **87**, 106–122.

- Eggler, D., Karimi, M., and Kessissoglou, N. (2019b). "Active acoustic cloaking in a convected flow field," *J. Acoust. Soc. Am.* **146**(1), 586–594.
- Elliott, S. J., Cheer, J., Choi, J.-W., and Kim, Y. (2012). "Robustness and regularization of personal audio systems," *IEEE Trans. Audio Speech Lang. Process.* **20**(7), 2123–2133.
- Euclid, E. (2012). *The Thirteen Books of the Elements* (Dover Publications, New York), Vol. 1.
- Fuller, C. C., Elliott, S., and Nelson, P. A. (1996). *Active Control of Vibration* (Academic Press, New York).
- Futhazar, G., Parnell, W. J., and Norris, A. N. (2015). "Active cloaking of flexural waves in thin plates," *J. Sound Vib.* **356**, 1–19.
- Guicking, D. (1990). "On the invention of active noise control by Paul Lueg," *J. Acoust. Soc. Am.* **87**(5), 2251–2254.
- Guicking, D. (2007). "Active control of sound and vibration: History—Fundamentals—State of the art," in *Oscillations, Waves and Interactions Sixty Years Drittes Physikalisches Institut A Festschrift* (Universitätsverlag Göttingen, Göttingen, Germany) pp. 107–138.
- House, C., Cheer, J., and Daley, S. (2020). "An experimental investigation into active structural acoustic cloaking of a flexible cylinder," *Appl. Acoust.* **170**, 107436.
- Lin, C., Lin, D., Eggler, D., and Kessissoglou, N. (2021). "Active acoustic cloaking and illusions of sound-hard bodies using the boundary element method," *J. Acoust. Soc. Am.* **149**(3), 1803–1812.
- Ma, Q., Mei, Z. L., Zhu, S. K., Jin, T. Y., and Cui, T. J. (2013). "Experiments on active cloaking and illusion for laplace equation," *Phys. Rev. Lett.* **111**(17), 173901.
- Martin, P. A. (2006). *107 Multiple Scattering: interaction of Time-Harmonic Waves with N Obstacles* (Cambridge University Press, Cambridge, UK).
- Miller, D. A. (2006). "On perfect cloaking," *Opt. Express* **14**(25), 12457–12466.
- Nelson, P. A., and Elliott, S. J. (1991). *Active Control of Sound* (Academic Press, New York).
- Norris, A. N. (2008). "Acoustic cloaking theory," *Proc. R Soc. A* **464**(2097), 2411–2434.
- Norris, A. N., Amirkulova, F. A., and Parnell, W. J. (2012). "Source amplitudes for active exterior cloaking," *Inverse Problems* **28**(10), 105002.
- Norris, A. N., Amirkulova, F. A., and Parnell, W. J. (2014). "Active elastodynamic cloaking," *Math. Mech. Solids* **19**(6), 603–625.
- O'Neill, J., Selsil, Ö., McPhedran, R., Movchan, A., and Movchan, N. (2015). "Active cloaking of inclusions for flexural waves in thin elastic plates," *Q. J. Mech. Appl. Math.* **68**(3), 263–288.
- O'Neill, J., Selsil, Ö., McPhedran, R., Movchan, A., Movchan, N., and Henderson Moggach, C. (2016). "Active cloaking of resonant coated inclusions for waves in membranes and Kirchhoff plates," *Q. J. Mech. Appl. Math.* **69**(2), 115–159.
- Onofrei, D., and Platt, E. (2018). "On the synthesis of acoustic sources with controllable near fields," *Wave Motion* **77**, 12–27.
- Schurig, D., Mock, J. J., Justice, B., Cummer, S. A., Pendry, J. B., Starr, A. F., and Smith, D. R. (2006). "Metamaterial electromagnetic cloak at microwave frequencies," *Science* **314**(5801), 977–980.
- Silveirinha, M. G., Alù, A., and Engheta, N. (2007). "Parallel-plate metamaterials for cloaking structures," *Phys. Rev. E* **75**(3), 036603.
- Varshalovich, D., Moskalev, A., and Khersonskii, V. (1988). "Description of rotation in terms of the Euler angles," in *Quantum Theory of Angular Momentum* (World Scientific, Singapore), pp. 21–23.
- Vasquez, F. G., Milton, G. W., and Onofrei, D. (2009a). "Active exterior cloaking for the 2D Laplace and Helmholtz equations," *Phys. Rev. Lett.* **103**(7), 073901.
- Vasquez, F. G., Milton, G. W., and Onofrei, D. (2009b). "Broadband exterior cloaking," *Opt. Express* **17**(17), 14800–14805.
- Vasquez, F. G., Milton, G. W., and Onofrei, D. (2011). "Exterior cloaking with active sources in two dimensional acoustics," *Wave Motion* **48**(6), 515–524.
- Vasquez, F. G., Milton, G. W., Onofrei, D., and Seppecher, P. (2013). "Transformation elastodynamics and active exterior acoustic cloaking," in *Acoustic Metamaterials* (Springer, New York), pp. 289–318.
- Wigner, E. (2012). *Group Theory: And Its Application to the Quantum Mechanics of Atomic Spectra* (Elsevier, Amsterdam), Vol. 5.
- Zheng, H., Xiao, J., Lai, Y., and Chan, C. (2010). "Exterior optical cloaking and illusions by using active sources: A boundary element perspective," *Phys. Rev. B* **81**(19), 195116.
- Zhang, S., Xia, C., and Fang, N. (2011). "Broadband acoustic cloak for ultrasound waves," *Phys. Rev. Lett.* **106**(2), 024301.